Formation times of electric-field domains in doped GaAs-AlAs superlattices

J. Kastrup

Paul-Drude-Institut für Festkörperelektronik, Hausvogteiplatz 5-7, D-10117 Berlin, Germany

F. Prengel

Institut für Theoretische Physik, Technische Universität Berlin, Hardenbergstrasse 36, D-10623 Berlin, Germany

H. T. Grahn and K. Ploog

Paul-Drude-Institut für Festkörperelektronik, Hausvogteiplatz 5-7, D-10117 Berlin, Germany

E. Schöll

Institut für Theoretische Physik, Technische Universität Berlin, Hardenbergstrasse 36, D-10623 Berlin, Germany

(Received 7 June 1995)

Electric-field domains in doped semiconductor superlattices lead to a series of stable branches in the current-voltage characteristics. The formation time of the domains is interpreted as the equilibration time of the system after the bias voltage is applied. Time-resolved current measurement techniques in conjunction with simulations are used to analyze the domain formation. Two different formation mechanisms are found. The investigated sample exhibits formation times from a few hundred nanoseconds up to several microseconds, depending on the applied voltage. For more strongly coupled superlattices much shorter formation times are expected.

Electric-field domains in GaAs-AlAs superlattices form as a consequence of the strongly nonlinear transport characteristic in an applied electric field.[1–5] While stable electric-field domains (EFDs) have been investigated rather extensively since their first observation, there are only a few reports on experiments[6,7] and calculations[8,9] targeting their transient behavior. Nevertheless, the time scales on which the electric-field domains form are of considerable importance for the assessment of the value of EFD structures as multistable memory devices which can store more than one bit "vertically."[10]

In this work we present measurements and simulations on the domain formation time indicating that it depends mainly on the tunneling time of the electrons between adjacent wells. Furthermore, the exact location of the accumulating domain boundary is shown to influence the formation time. Simulations and measurements of the current in voltage turn-on experiments show a series of spikes during the formation process which are associated with a well-by-well hopping of the domain boundary through the superlattice. This allows us to determine the location of the boundary in the superlattice resulting in a depth resolution of about one superlattice period.

The superlattice consists of 40 periods of 9-nm GaAs wells and 4-nm AlAs barriers with a two-dimensional (2D) Si-doping density of $N_{2D}=1.5\times10^{11}$ cm^{-2} inside the wells. It has been grown by molecular beam epitaxy between two highly Si-doped n^+-Al$_{0.5}$Ga$_{0.5}$As contact layers with doping densities of 2×10^{18} cm^{-3}. The samples are structured into mesas of 120 μm diameter with Cr/Au contacts on top and AuGe/Ni contacts on the substrate side. For further details on this sample see Ref. 10. All experiments are performed at 5 K in a He-flow cryostat using high-frequency coaxial cables with a bandwidth of 20 GHz. The voltage pulses are generated with a Wavetek 50 MHz pulse/function generator

(model 81), and the time dependent current is detected with a Tektronix sampling oscilloscope CSA 803 using the sampling head SD-32. Throughout this paper we present data obtained with voltage pulses of 5 μs width and 10 μs period. Pulse width and period have been chosen sufficiently long to allow the field distribution inside the superlattice to stabilize after the voltage is turned on, and to reset the field and charge distribution before the next pulse arrives.

The numerical simulations have been performed on the basis of a phenomenological one-dimensional model which is described in the Appendix. The parameters have been chosen such that good quantitative agreement between calculated and measured static *I-V* characteristics is achieved.

The time-averaged *I-V* characteristics has been published in Ref. 10. The sample exhibits electric-field domains between -0.5 and -4.5 V. Figure 1 shows the time-resolved current responses to applied voltages below (-0.3 V), inside (-3 V), and above the domain regime (-5.5 V). All three
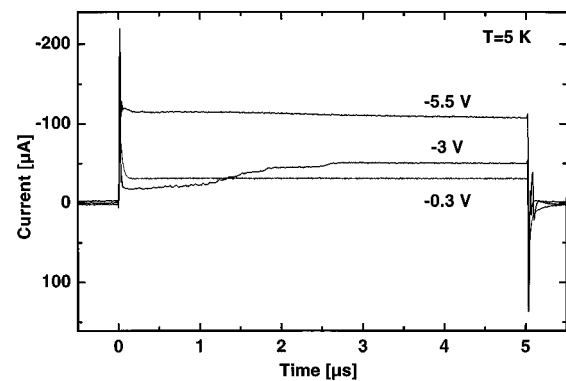

FIG. 1. Measured time-resolved current response to applied voltages inside (-3 V) and outside (-0.3 and -5.5 V) the domain regime.
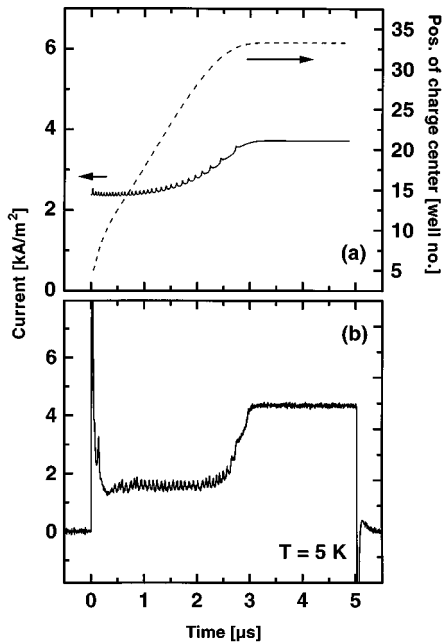
FIG. 2. (a) Calculated current response to an applied voltage step from 0 to -1 V exhibiting well-to-well hopping spikes. The dashed line shows the center of the charge accumulation layer as it drifts through the superlattice into its stable position in well no. 34. (b) Experimental current response to an applied voltage of -1 V. The turn-on and turn-off spikes are cut off to enhance the visibility of the well-to-well hopping spikes.
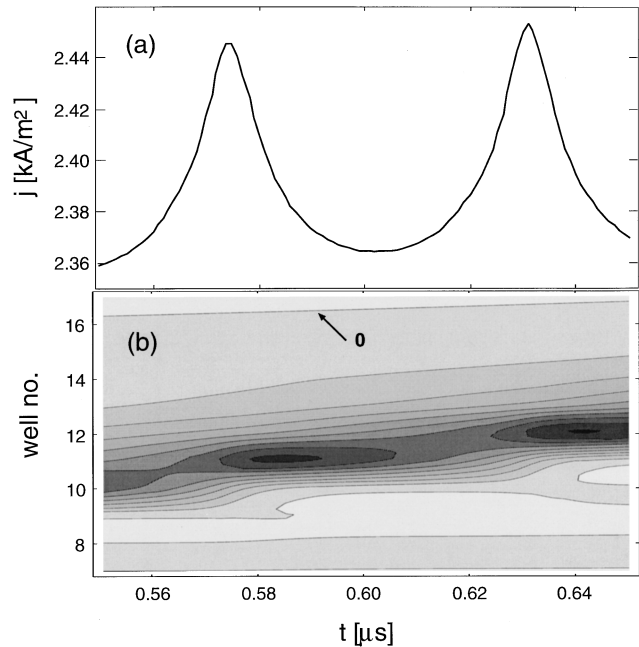

FIG. 3. (a) Enlarged section of the calculated current in Fig. 2(a). (b) Contour plot of the calculated effective charge density $n_1^{(k)} + n_2^{(k)} - N_D^{(k)}$ vs time in wells no. 7–17. Darker shading corresponds to higher densities; consecutive isolines differ by 10^{16} cm^{-3}. The line marked "0" denotes charge neutrality.

curves begin (and end) with a sharp spike when the voltage is turned on (or off). These spikes are due to the displacement current $\varepsilon \dot{F}$ of the sample (where ε denotes the permittivity and F the field), when a voltage step occurs, and reflect mainly the shape of the pulse edges. The response above and below the domain region instantaneously leads to the current that is expected from the static I-V characteristic.[10] However, the response to a -3 V pulse shows a drastically different time dependent behavior. After the initial spike the current decreases to a minimum level of about 15 μA before it rises in a series of steps to a stable level at 50 μA. In the low-level region the current displays a series of small spikes which, as the current rises, lead to the steplike features.

Figure 2 shows the calculated and measured time dependence of the current density when the voltage is switched from 0 to -1 V. In Fig. 2(a) the switching process is realized by calculating the evolution of the field distribution starting with a homogeneous field of the desired strength. Therefore the experimentally observed sharp turn-on (and turn-off) spikes are not reproduced by the calculation. The dashed line shows the position of the charge accumulation layer during the formation process. Figure 2(b) shows the corresponding experimental result which has been obtained by recording the time-resolved current response to a voltage pulse of -1 V. One clearly sees the good quantitative agreement with respect to both the time scale and the detailed shape of the curves. Special attention should be devoted to the small current spikes. The simulations show that they are due to the well-to-well hopping of a charge monopole which, from the investigation of static field domains in superlattices, is

known to form the boundary between the low- and high-field domains. In Fig. 3(a) we show an enlarged section of Fig. 2(a) for 0.55 μs$<t<$0.65 μs, and in Fig. 3(b) the corresponding contour plot of the charge density for the wells no. 7–17. At $t_0 = 0.585$ μs, the charge monopole is located in the 11th well, and it moves to well no. 12 between t_0 and $t_1 = 0.64$ μs. The current peaks occur when the gradient of the contour associated with a density of 1×10^{16} cm^{-3} exhibits a maximum, which corresponds to the extension of the low-field domain by one well.

Thus stable domains are formed in the following way. Immediately after the voltage is turned on, the electric field is constant throughout the sample. Then, a charge monopole forms at the cathode (well no. 1) and moves towards the anode hopping from well to well, until it reaches a location which ensures a stable field distribution.

Figure 4(a) shows the measured (full squares) and calculated (open circles) formation times for voltages inside the domain regime. The measured times have been determined from a series of time-resolved voltage turn-on measurements similar to the one shown in Fig. 2(b). In order to have a simple criterion, the formation time is interpreted as the time it takes for the current to cross a threshold level of 35 μA. We see that after a sharp initial increase the formation time reaches a maximum of roughly 3 μs at about -1 V and then gradually decreases towards the end of the domain region.

For the calculated times, a similar criterion has been used with a threshold current density of 3.5 kA/m^2. The quantitative agreement is satisfactory, although the curves differ in some details. The simulations show that there is an influence of the shape of the drift-velocity vs field $[v(F)]$ characteristic in the plateau region *between* the resonant peaks [shown
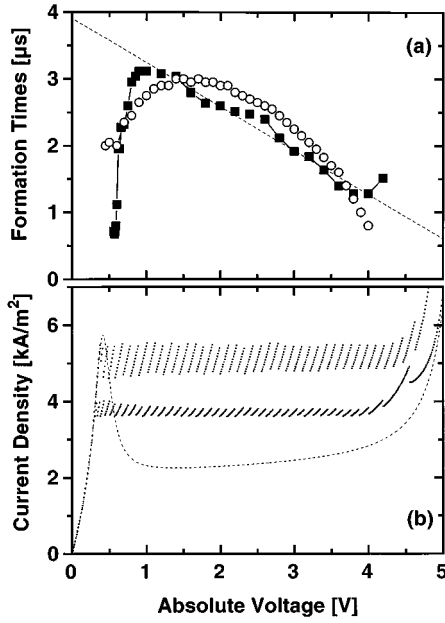
FIG. 4. (a) Experimental (full squares) and theoretical (open circles) formation times vs applied voltages in the plateau region. The dashed line shows the linear regression for the experimental data points between -1 and -3 V. (b) Calculated I-V characteristics for up sweep (upper dotted curve), down sweep (lower dotted curve), and uniform field distribution (dashed curve) reflecting the drift-velocity vs field relation $v(F)$.

in Fig. 4(b) as calculated] on the dynamics of domain formation. Therefore the calculated formation times develop somewhat differently with voltage. From the series of current spikes in Fig. 2(b) the time it takes for the domain boundary to tunnel from one well to the next is estimated to be about 60 ns. Assuming that the boundary would come to rest in well number 40, the longest formation time would be 40×60 ns $= 2.4$ μs. The longest formation times measured are about 3 μs because the last few well-to-well transitions often take significantly longer than 60 ns (cf. Fig. 2). These last few wells represent quasistable positions for the domain boundary so that the transition time to the final position depends critically on small disturbances. As it is shown in Ref. 10, in certain voltage regions there may be more than one stable position for the domain boundary, which implies that the transition time becomes infinitely long. Note that the presented set of data points only shows the principal behavior of the formation times. However, the previous arguments indicate that there will be a local modulation, which depends on the actual position of the stable operating point.

At this point it is worthwhile to note that beyond -1 V the formation time τ_f decreases almost linearly (experimental curve) with $d\tau_f/dV = 660$ ns/V. In this voltage regime the domain boundary has to propagate from the cathode into its final position so that the formation time decreases the closer the final position of the boundary is to the cathode. With increasing absolute voltage the stable high-field domain originating from the anode extends in fact further towards the cathode. In Ref. 10 it is shown that the voltage drop in the high-field region is about $\Delta V = 110$ mV/well, leading to an average transition time of $d\tau_f/dV\Delta V = 73$ ns/well, which

is close to the well-to-well propagation time of 60 ns which we found from the current spikes. Even though this simple comparison ignores the fact that the well-to-well hopping times change somewhat during the formation process, it shows clearly that the origin of the decreasing formation time is the decreasing propagation distance of the domain boundary at larger absolute voltages. Between 0 and -1 V the formation time becomes shorter than the propagation time, indicating that a different formation mechanism exists. This is supported by preliminary calculations which have shown that in this regime the domain boundary forms inside the superlattice close to its final position, i.e., in place. Comparing the calculated formation times of Fig. 4(a) and the calculated $v(F)$ curve [dashed line in Fig. 4(b)] we note that an increase of the formation time with increasing voltage is only observed in the negative differential velocity regime of the $v(F)$ curve. Hence we conclude that the in-place formation mechanism is closely related to negative differential drift velocity of the first resonance.

In summary, we have demonstrated that the formation time of electric-field domains in doped superlattices depends critically on the coupling which defines the well-to-well propagation time for the domain boundary. However, the formation time also depends on the applied voltage, which in turn determines the final location of the stable domain boundary inside the superlattice. Theory and experiment show that two different formation mechanisms exist. While in the negative differential velocity region of the $v(F)$ curve the domain boundary forms in place, at higher voltages it propagates into the superlattice from the cathode well by well. Because the well-to-well transition time can be varied over several orders of magnitude by changing the barrier widths, samples with much shorter formation times can be realized by using thinner barriers.

APPENDIX: THE MODEL USED IN THE SIMULATIONS

The model is similar to that developed in Ref. 11. Here the doping density is chosen sufficiently large so that self-sustained oscillations[9] do not occur. Our superlattice is made of $N = 40$ quantum wells of width $l = 9$ nm (the GaAs layers) and depth $\Delta E_c = 982$ meV (the conduction band discontinuity between GaAs and AlAs), which are weakly coupled by barriers of width $b = 4$ nm (the AlAs layers). The superlattice period is thus $d = l + b = 13$ nm. We then calculate the two lowest energy levels E_1 and E_2 of the isolated quantum wells and the corresponding wave functions ψ_1 and ψ_2. Dynamic quantities are the three-dimensional electron densities $n_1^{(k)}$ and $n_2^{(k)}$ ascribed to levels 1 and 2 in the kth well. The electric field $F^{(k)}$ between wells no. $(k-1)$ and (k) is assumed to be piecewise constant. From Gauss's law we have

$$e(n_1^{(k)} + n_2^{(k)} - N_D^{(k)}) = \varepsilon \frac{F^{(k+1)} - F^{(k)}}{l}, \quad (A1)$$

where $N_D^{(k)}$ is the background doping density in the kth well, ε is the dielectric permittivity of the well material, and e is the unit charge.

The doping density $N_D^{(k)}$ is allowed to fluctuate[12] around a mean value of $N_D = 1.67 \times 10^{17}$ cm^{-3}:

$$N_D^{(k)} = (1 + \alpha^{(k)}) N_D,$$

with random numbers $\alpha^{(k)}$ chosen with equal probability from an interval $[-0.01, 0.01]$.

Contacts are modeled by additional wells 0 and $N+1$ with

$$n_1^{(0)} = n_1^{(N+1)} = 2N_D, \quad n_2^{(0)} = n_2^{(N+1)} = 0.$$

Transport between level i in the kth well and level i' in the k'th well (where $i, i' = 1, 2$, $k = 1, \ldots, N$ and $k' = k \pm 1$) is given by tunneling rates $\omega_{ii'}^{(k \to k')}$:

$$\omega_{ii}^{(k-1 \to k)}(F^{(k)}) = \frac{2\pi}{\hbar} |V_{ii}|^2 \frac{\Gamma}{\Gamma^2 + (edF^{(k)} - E_{11}^*)^2} + \theta(F^{(k)}) \left(\frac{edF^{(k)}}{E_{11}^*} \theta(E_{11}^* - edF^{(k)}) + \theta(edF^{(k)} - E_{11}^*) \right)$$

$$\times C_{nr} \frac{E_i}{2\pi\hbar} \exp\left[-\frac{2b}{\hbar} \sqrt{2m^*(\Delta E_c - E_i)} \right], \tag{A2}$$

$$\omega_{ii}^{(k \to k-1)}(F^{(k)}) = \omega_{ii}^{(k-1 \to k)}(-F^{(k)}) \quad (i = 1, 2), \tag{A3}$$

$$\omega_{12}^{(k-1 \to k)}(F^{(k)}) = \frac{2\pi}{\hbar} |V_{12}|^2 \frac{\Gamma}{\Gamma^2 + (edF^{(k)} - E_{12}^*)^2}, \quad \omega_{12}^{(k \to k-1)}(F^{(k)}) = \omega_{12}^{(k-1 \to k)}(-F^{(k)}), \tag{A4}$$

$$\omega_{21}^{(k-1 \to k)}(F^{(k)}) = \frac{2\pi}{\hbar} |V_{21}|^2 \frac{\Gamma}{\Gamma^2 + (edF^{(k)} + E_{12}^*)^2}, \quad \omega_{21}^{(k \to k-1)}(F^{(k)}) = \omega_{21}^{(k-1 \to k)}(-F^{(k)}). \tag{A5}$$

Here, resonant tunneling with a Lorentzian shape is described by matrix elements $V_{11} = 4.23 \times 10^{-6} \Delta E_c$, $V_{22} = 2.62 \times 10^{-5} \Delta E_c$, $V_{12} = 1.44 \times 10^{-5} \Delta E_c$, and $V_{21} = 3.05 \times 10^{-5} \Delta E_c$, a peak width $\Gamma = 3.3$ meV, as well as peak positions $E_{11}^* = 10$ meV and $E_{12}^* = E_2 - E_1 = 133$ meV for the first and second peak, respectively.

In comparison with the experimental values we note that some of the parameters may seem somewhat unrealistic. For example, the value for E_{11}^*, which in a microscopic model reflects miniband width, is clearly larger than the expected miniband width (here : < 0.1 meV). However, for the "fitted" phenomenological model presented in this work the values E_{11}^*, E_{12}^*, and Γ reflect the *positions and shape of the maxima* in the experimental current-voltage curve which includes not only possible irregularities of the superlattice, but also the crucial influence of the contacts.

The plateau region between the resonant peaks is modeled by a "nonresonant" component in the WKB approximation which is incorporated into ω_{ii} and contains the effective electron mass $m^* = 0.15 m_e$ in AlAs and a fit factor $C_{nr} = 4$; θ is the Heaviside function.

The current density between the subbands is then $j_{ii'}^{(k \to k')} = e n_i^{(k)} l \omega_{ii'}^{(k \to k')}$, and the overall current density across barrier (k) is

$$j(F^{(k)}) = \sum_{i=1,2} (j_{1i}^{(k-1 \to k)} + j_{2i}^{(k-1 \to k)}$$

$$- j_{1i}^{(k \to k-1)} - j_{2i}^{(k \to k-1)}). \tag{A6}$$

Additionally, intersubband relaxation between levels 2

and 1 inside each well (k) is assumed to take place with a relaxation time $\tau = 10^{-11}$ s. The value of τ has been chosen relatively large in order to increase the computation speed. This does not affect the outcome of the simulations because τ is still much shorter than the tunneling times.

We then have a set of rate equations for the electron densities $n_i^{(k)}$,

$$\dot{n}_1^{(k)} = \frac{n_2^{(k)}}{\tau} + \frac{1}{el} \left[\sum_{i=1,2} \sum_{m=\pm 1} (j_{i1}^{(k+m \to k)} - j_{1i}^{(k \to k+m)}) \right], \tag{A7}$$

$$\dot{n}_2^{(k)} = -\frac{n_2^{(k)}}{\tau} + \frac{1}{el} \left[\sum_{i=1,2} \sum_{m=\pm 1} (j_{i2}^{(k+m \to k)} - j_{2i}^{(k \to k+m)}) \right], \tag{A8}$$

which becomes complete by the boundary condition

$$\sum_{k=1}^{N+1} F^{(k)} = V/d, \tag{A9}$$

where V denotes the applied voltage.

The quantity corresponding to the experimentally measured current I is the effective current density

$$j(t) \equiv j(F^{(k)}) + \varepsilon \dot{F}^{(k)}, \tag{A10}$$

which is the sum of the particle current $j(F^{(k)})$ and the displacement current $\varepsilon \dot{F}^{(k)}$ across barrier (k). Thus $j(t)$ is independent of k and denotes the current density which is shown in the simulation results throughout this work.

[1] L. Esaki and L. L. Chang, Phys. Rev. Lett. **33**, 495 (1974).

[2] K. K. Choi, B. F. Levine, R. Malik, J. Walker, and C. G. Bethea, Phys. Rev. B **35**, 4172 (1987).

[3] S. H. Kwok, R. Merlin, H. T. Grahn, and K. Ploog, Phys. Rev. B **50**, 2007 (1994).

[4] Y. Zhang, X. Yang, W. Liu, P. Zhang, and D. Jiang, Appl. Phys. Lett. **65**, 1148 (1994).

[5] Z. Y. Han, S. F. Yoon, K. Radhakrishnan, and D. H. Zhang, Appl. Phys. Lett. **66**, 1120 (1995).

[6] S. H. Kwok, T. B. Norris, L. L. Bonilla, J. Galán, J. A. Cuesta, F. C. Martínez, J. Molera, H. T. Grahn, K. Ploog, and R. Merlin, Phys. Rev. B **51**, 10 171 (1995).

[7] H. T. Grahn, R. Klann, and W. W. Rühle, in *Proceedings of the 22nd International Conference on the Physics of Semiconduc-tors*, edited by D. J. Lockwood (World Scientific, Singapore, 1995), p. 1169.

[8] L. L. Bonilla, J. Galán, J. A. Cuesta, F. C. Martínez, and J. M. Molera, Phys. Rev. B **50**, 8644 (1994).

[9] A. Wacker, F. Prengel, and E. Schöll, in *Proceedings of the 22nd International Conference on the Physics of Semiconductors*, Ref. 7, p. 1075.

[10] J. Kastrup, H. T. Grahn, K. Ploog, F. Prengel, A. Wacker, and E. Schöll, Appl. Phys. Lett. **65**, 1808 (1994).

[11] F. Prengel, A. Wacker, and E. Schöll, Phys. Rev. B **50**, 1705 (1994).

[12] A. Wacker, G. Schwarz, F. Prengel, E. Schöll, J. Kastrup, and H. T. Grahn, Phys. Rev. B **52**, 13 788 (1995).